Oligodendroglial NMDA Receptors Regulate Glucose Import and Axonal Energy Metabolism

Aiman S. Saab[1,2,3], **Iva D. Tzvetavona**[1], **Andrea Trevisiol**[1], **Selva Baltan**[4], **Payam Dibaj**[1], **Kathrin Kusch**[1], **Wiebke Möbius**[1,5], **Bianka Goetze**[6], **Hannah M. Jahn**[1,2], **Wenhui Huang**[1,2], **Heinz Steffens**[7,8], **Eike D. Schomburg**[7], **Alberto Pérez-Samartín**[9], **Fernando Pérez-Cerdá**[9], **Davood Bakhtiari**[5,10], **Carlos Matute**[9], **Siegrid Löwel**[6], **Christian Griesinger**[5,10], **Johannes Hirrlinger**[1,11], **Frank Kirchhoff**[1,2,5,*], **Klaus-Armin Nave**[1,5,*]

[1]Max Planck Institute of Experimental Medicine, Department of Neurogenetics, Göttingen 37075, Germany

[2]Center for Integrative Physiology and Molecular Medicine, Molecular Physiology, University of Saarland, Homburg 66421, Germany

[3]University of Zurich, Institute of Pharmacology and Toxicology, 8057 Zurich, Switzerland

[4]Lerner Research Institute, Cleveland Clinic, Department of Neurosciences, Cleveland, OH 44195, USA

[5]Center Nanoscale Microscopy and Molecular Physiology of the Brain (CNMPB), 37073 Göttingen, Germany

[6]Bernstein Focus for Neurotechnology (BFNT) and School of Biology, Department of Systems Neuroscience, University of Göttingen, 37075 Göttingen, Germany

[7]Institute of Physiology, University of Göttingen, 37073 Göttingen, Germany

[8]Max Planck Institute for Biophysical Chemistry, Department of NanoBiophotonics, 37077 Göttingen, Germany

[9]Universidad del País Vasco, CIBERNED and Departamento de Neurociencias and Achucarro Basque Center for Neuroscience, Leioa 48940, Spain

[10]Department of NMR Based Structural Biology, Max Planck Institute for Biophysical Chemistry, 37077 Göttingen, Germany

[*]Correspondence: frank.kirchhoff@uks.eu (F.K.), nave@em.mpg.de (K.-A.N.).

[11]Carl-Ludwig-Institute for Physiology, Faculty of Medicine, University of Leipzig, 04103 Leipzig, Germany

SUMMARY

Oligodendrocytes make myelin and support axons metabolically with lactate. However, it is unknown how glucose utilization and glycolysis are adapted to the different axonal energy demands. Spiking axons release glutamate and oligodendrocytes express NMDA receptors of unknown function. Here we show that the stimulation of oligodendroglial NMDA receptors mobilizes glucose transporter GLUT1, leading to its incorporation into the myelin compartment in vivo. When myelinated optic nerves from conditional NMDA receptor mutants are challenged with transient oxygen-glucose deprivation, they show a reduced functional recovery when returned to oxygen-glucose but are indistinguishable from wild-type when provided with oxygen-lactate. Moreover, the functional integrity of isolated optic nerves, which are electrically silent, is extended by preincubation with NMDA, mimicking axonal activity, and shortened by NMDA receptor blockers. This reveals a novel aspect of neuronal energy metabolism in which activity-dependent glutamate release enhances oligodendroglial glucose uptake and glycolytic support of fast spiking axons.

In Brief

Saab et al. identify a novel feature of axonal metabolic support. Activation of oligodendroglial NMDA receptors stimulates GLUT1 export and release of lactate. Targeted inactivation of oligodendroglial NMDA receptors in vivo impairs axonal energy metabolism and causes late-onset axonopathy.

INTRODUCTION

Oligodendrocytes, best known for making myelin (Emery, 2010; Nave and Werner, 2014), also support the survival of myelinated axons (Griffiths et al., 1998; Kassmann et al., 2007; Lappe-Siefke et al., 2003). Myelin is assembled as a spiral extension of oligodendroglial cell membrane, which requires vesicular transport of membrane material through non-compacted cytosolic channels to the growing tip (Snaidero et al., 2014). In mature myelin, a system of nanometer-wide "myelinic channels" is left behind, the dynamics and dimensions of which were only appreciated with the application of high-pressure freezing (HPF) electron microscopy (Snaidero et al., 2014).

Recently, the identification of metabolic coupling between oligodendrocytes and the axonal compartment, with glycolytic oligodendrocytes providing lactate to axons for aerobic ATP production (Fünfschilling et al., 2012; Lee et al., 2012), has introduced a new paradigm for the interaction of axons and their associated glial cells. However, the concept of glycolytic support by oligodendrocytes (Morrison et al., 2013; Saab et al., 2013) raises the question of how glucose utilization is quantitatively regulated. Since the average spike count rate is the key determinant of axonal ATP consumption, oligodendrocytes need to "know" the spiking activity of myelinated axons, which can differ greatly in vivo (Barry, 2015; Perge et al., 2012). The constitutive overproduction of lactate would result in lactic acidosis, detrimental

for white matter function. A plausible preventive mechanism would be that oligodendrocytes "learn" their association with fast spiking axons to adapt their own energy metabolism.

Like unmyelinated axons (Kukley et al., 2007; Wake et al., 2011; Ziskin et al., 2007) also myelinated axons release glutamate upon spiking, which induces calcium elevations in myelin (Micu et al., 2016). Oligodendrocytes could take trace amounts of glutamate as a proxy for axonal spiking activity and energy needs. Indeed, periaxonal spaces underneath myelin are narrow (<50 nm), and glutamate could reach high local concentrations (Stys, 2011).

Oligodendrocytes express different glutamate receptors, including NMDA receptors of unknown function (Káradóttir et al., 2005; Micu et al., 2006; Salter and Fern, 2005). A role for NMDA receptor signaling in oligodendrocyte differentiation and promoting myelination has been suggested, based on in vitro observations (Li et al., 2013; Lundgaard et al., 2013), which is compatible with neuronal activity stimulating OPC proliferation and myelination in vivo (Gibson et al., 2014; Liu et al., 2012). Recently, axonal activity was shown to induce NMDA receptor-mediated calcium increases in myelin, indicating that adult oligodendrocytes have functional NMDA receptors (Micu et al., 2016). However, conditional mouse mutants lacking this receptor from OPC reveal no major abnormality (De Biase et al., 2011; Guo et al., 2012).

NR1 is the obligate subunit of tetrameric NMDA receptors, and expression of its gene (*Grin1*) is higher in OPC than in mature oligodendrocytes (Zhang et al., 2014) but remains detectable throughout adult life (this study). Here, we tested the hypothesis that NMDA receptor signaling to oligodendrocytes is the missing link in coupling axonal activity and ATP consumption to oligodendroglial glucose utilization and lactate supply.

RESULTS

NMDA Receptor Activation Triggers GLUT1 Surface Expression and Enhances Glucose Import in Cultured Oligodendrocytes

Oligodendroglial GLUT1 was localized to intracellular compartments and primary processes (but only weakly to secondary and tertiary processes) and immature myelin membranes (Figure 1A, top). Cultured neurons mobilize glucose transporter GLUT3 in response to glutamate (Ferreira et al., 2011). We therefore asked whether GLUT1, the predominant transporter of oligodendrocytes and astrocytes (Zhang et al., 2014), behaves similarly.

Remarkably, treatment with NMDA triggered GLUT1 redistribution in oligodendrocytes within 30 min, leading to apparent surface expression (Figure 1A, middle) that was efficiently blocked by D-(−)-2-amino-5-phosphonopentanoic acid (D-AP5) (Figures 1A, bottom, and 1C). In contrast, monocarboxylate transporter MCT1 distribution was unaffected by NMDA (Figures S1A and S1B). To confirm that NMDA promotes membrane insertion of GLUT1, we performed biotinylation assays with immunopanned oligodendrocytes (Figure 1B), revealing a 2-fold GLUT1 increase at the cell surface following 30 min NMDA stimulation (Figure 1D), whereas the abundance of MCT1 was the same. To determine functional GLUT1 insertion, we expressed a glucose sensor

(Takanaga et al., 2008) in transfected oligodendrocytes (Figure 1E). Activation of NMDA receptors caused a significantly increased FRET signal that was abolished by 7-CKA and D-AP5, which block both the glycinergic and glutamatergic NMDA receptor binding sites, respectively (Figure 1F). Calibration of the FRET sensor allowed the measurement of cytosolic glucose in oligodendrocytes, i.e., 0.56 ± 0.04 mM at baseline and 1.85 ± 0.24 mM following NMDA receptor stimulation (Figure 1G). Finally, we used immunopanned oligodendrocytes and quantified the uptake of 2-deoxyglucose (2DG) to confirm that NMDA elevates glucose import (Figure 1H). In these experiments, elevated glucose was not caused by inhibition of glycolysis because the release of lactate was simultaneously enhanced. By NMR spectroscopy, we calculated a $24\% \pm 4\%$ increase of U-^{13}C-lactate release originating from U-^{13}C$_6$-labeled glucose (Figures 1I–1K). As expected, lactate release from cultured oligodendrocytes relies on glucose availability (Figures S1C and S1D). However, NMDA-stimulated lactate release was unexpected (Figures 1I–1K and S1E) because basic metabolic demands did not change, and there were no signs of oligodendrocyte death (Figure S1F). Most likely, membrane repolarization (triggered by NMDA receptor signaling and ion influx) consumes the additional ATP and leads to more glycolysis with lactate release.

Myelination In Vivo in the Absence of Oligodendroglial NMDA Receptors

Glucose is a major carbon source for lipid precursor metabolites, which are rate-limiting for myelination (Rinholm et al., 2011). In vivo, reduced glutamate signaling might thus affect myelination during development. To study oligodendroglial NMDA receptor function, we crossed mice with a floxed *NR1* allele (Tsien et al., 1996) to *Cnp1*$^{Cre/+}$ mice (Lappe-Siefke et al., 2003). NR1 (gene symbol *Grin1*) encodes the obligatory subunit of functional NMDA receptors (Tsien et al., 1996).

In *Grin1*$^{flox/flox}$**Cnp1*$^{Cre/+}$ mice (hereafter termed NR1 mutant or cKO, with *Grin1*$^{flox/flox}$**Cnp1*$^{+/+}$ and *Grin1*$^{flox/+}$**Cnp1*$^{Cre/+}$ being controls), NR1 was lost by immunostaining, as shown for optic nerve (Figures 2A, 2B, and S2A), by qPCR of genomic DNA and by western blot analysis (Figures 2C and 2D). Recombination analysis revealed that at P5, when the optic nerve is already populated with oligodendroglial precursor cells (OPCs), loss of the floxed allele was not yet significant. However, at P10, when many oligodendrocytes had matured and express Cnp1, about one-third of the floxed alleles were excised, and recombination reached $62\% \pm 8\%$ at P96, when myelination is completed, matching the expected proportion of oligodendrocyte in adult optic nerves (Miller et al., 1985). Cre-mediated reporter expression in optic nerves demonstrated that virtually all recombined cells were of oligodendroglial origin (Figures S2B and S2C). NR1 expression in astrocytes and OPCs could account for the remaining 40% NR1 signal of whole optic nerve immunostainings (Figure 2B) or protein lysates (Figure 2D).

In purified myelin from mutant brains, we found a strong reduction of GLUT1 (but not MCT1) compared to controls (Figures 2E, 2F, S1G, and S1H), whereas total tissue GLUT1 was unchanged in NR1 mutants. By immunogold labeling of mature optic nerves, GLUT1 was localized in the myelin sheath, in the outer tongue, and in the paranodal loops (Figure 2G), well positioned for functional glucose uptake into the system of myelinic channels.

GLUT1 abundance in myelin sheaths of optic nerve axons was reduced by 80% in NR1 mutants compared to littermate controls (Figures 2H), in line with its NR1-dependent mobilization in cultured oligodendrocytes.

GLUT1 mRNA is more abundant in mature oligodendrocytes than in precursor cells (Zhang et al., 2014). From CNS white matter samples, we amplified equal amounts of GLUT1 and MCT1 cDNA when comparing mutants and controls, indicating that NMDA receptor signaling does not regulate GLUT1 at the level of gene expression (Figure S1I). Interestingly, we localized MCT1 by immuno-electron microscopy at both the outer and inner tongue of myelin (Figure 2I). Thus, lactate transporters are strategically positioned for taking up and supplying glycolysis products (Fünfschilling et al., 2012; Lee et al., 2012).

Phenotypically, mutant mice were normally developed with functional white matter tracts, as shown for the optic nerve (Figure S3), and are long-lived. This suggests that NMDA receptors are not essential for myelination per se, in agreement with earlier reports (De Biase et al., 2011; Guo et al., 2012). However, the paucity of GLUT1 in myelin (Figures 2E, 2F, and 2H) suggested reduced glucose import, which could affect the rate of myelin growth that is metabolically controlled (Rinholm et al., 2011). In the rodent optic nerve, the highest myelination rate occurs during the third postnatal week (Hildebrand and Waxman, 1984) and predicts the highest demands for glucose as a carbon source for lipid synthesis at this time. Indeed, by EM we noted at ages P18–P20 that myelin was thinner, with fewer myelinated axons in the mutant optic nerves (Figures 3B and 3D–3G). This difference was only transient as adult (P70) NR1 mutant optic nerves "catch up" and exhibit a normal myelin sheath thickness (Figures 3C, 3H, and 3I).

Functional Analysis of Myelinated Axons

To study function, we assessed optic nerve conduction at different stages of development by recording compound action potentials (CAPs) ex vivo, comparing NR1 mutant and controls (Figure S4). CAP profiles revealed a transiently reduced conduction velocity, again only at the peak of myelination (age P19–P21) and mainly affecting small caliber axons (Figures S4D–S4F). These are best explained by the delay of CNS myelination (Figures 3D–3I), as nerve caliber and axon numbers were normal (Figures S4J and S4K). The developmental delay of myelination in NR1 mutant optic nerves fits well the unexplained observation that demyelinating lesions repair less well when NMDA receptors are blocked (Li et al., 2013; Lundgaard et al., 2013).

Next, we examined myelinated optic nerves under metabolic stress for their ability to recover from transient oxygen-glucose deprivation (OGD), a well-established model of acute ischemia (Tekkök et al., 2007). Optic nerves were acutely isolated and CAPs were recorded ex vivo (Figure 4A, top). In these experiments, all optic nerves maintained conductivity (defined as "CAP area" of 1.0) and, within minutes after OGD onset, displayed block of nerve conduction, as illustrated by the rapid decline of CAP area (Figures 4A and 4B). When re-perfused 60 min later using oxygenated artificial cerebrospinal fluid (ACSF, 10 mM glucose), we determined some persistent loss of conduction in wild-type nerves, a Ca^{2+}-dependent damage to axons (Tekkök et al., 2007). Surprisingly, in NR1 mutant nerves the recovery of axon function was further reduced by 50% (Figures 4C). NMDA-

receptor-mediated excitotoxicity in oligodendrocytes (Káradóttir et al., 2005; Micu et al., 2006; Salter and Fern, 2005) may not be the main mechanism causing myelin damage (Hamilton et al., 2016). Indeed, ultrastructural damage following OGD alone, such as myelin delamination, was the same in NR1 mutants and controls (Figure S5A). Thus, further loss of axonal conductivity was not caused by more severe myelin injury, but rather by less-efficient axonal recovery from the metabolic stress of OGD. Importantly, axonal recovery after OGD was normal prior to age P10 (Figure S6A), suggesting that axons require oligodendroglial support mostly after myelination, which limits rapid axonal access to extracellular metabolites (Nave, 2010).

Causality of NMDA Receptor Signaling and Glucose Metabolism in Axonal Support

To demonstrate causality between oligodendroglial glucose metabolism and axonal recovery, we asked whether lactate, permeating through MCT1 (Figures 2I), can replace glucose as an energy source and restore conduction independent of prior NMDA receptor signaling. As predicted, using lactate-containing ACSF for reperfusion, optic nerves from NR1 mutants recovered as well as control nerves and even better than in the presence of glucose (Figures 4D and 4E). This confirms that axons readily use lactate for ATP generation (Fünfschilling et al., 2012; Lee et al., 2012; Tekkök et al., 2005; Wyss et al., 2011). More importantly, it also proves that optic nerves in NR1 mutants are not per se more susceptible to axonal injury. We confirmed this experimentally with MOG-induced experimental allergic encephalomyelitis (EAE), associated with secondary axonal dysfunction. Here, we found no difference in the onset of EAE symptoms or in clinical severity (Figures S5B–S5D), as indicated earlier (Guo et al., 2012; Matute, 2010).

During OGD, abnormal Ca^{2+} entry into the axonal compartment triggers axon loss probably resulting from excessive glutamate signaling caused by reversal of glutamate transporters (Stirling and Stys, 2010; Tekkök et al., 2007). Indeed, in the absence of free extracellular Ca^{2+}, the axonal recovery was almost 100% in control nerves yet remained significantly impaired in NR1 mutants (Figures S6E and S6F). Thus, glucose uptake by oligodendrocytes is critical to reenergize axons independent of Ca^{2+}-mediated damage.

We suggest that NMDA receptor signaling to oligodendrocytes enhances incorporation of GLUT1 into oligodendroglial and myelin membranes (providing "hardware" of glycolytic support), specifically around axons of higher electrical activity. Interestingly, when optic nerves were acutely isolated from wild-type mice and tested an hour later, the prior application of D-AP5, 7CKA, or MK801 (30 min before the onset of OGD) did not visibly reduce axonal recovery from OGD (Figure S6F), in line with older reports (Tekkök et al., 2007). This is no contradiction to the mutant phenotype in vivo, however, because development and pharmacology operate at different timescales, and it could take hours or days to lose functionally exposed GLUT1 from the myelin compartment. Indeed, wild-type optic nerves maintained for an extended time ex vivo, and then tested for conductivity, revealed an intriguing effect of both NMDA and NMDA receptor blockers. In the presence of glucose and oxygen, their basic conduction properties appeared unchanged after 16 hr (Figure S6G). We then studied axon function under metabolic challenge but chose a more physiological and graded paradigm than OGD. Optic nerves were stimulated by short bursts

with a gradual increase in frequency (between 1 and 100 Hz). As expected, the recorded CAPs declined as a function of increasing frequency (Figures 4F). Interestingly, when nerves were pre-incubated for 16 hr in the presence of 100 μM NMDA/Gly (mimicking glutamate release from spiking axons), high-frequency conductivity was much better maintained (Figure 4F). For example, NMDA-stimulated nerves appeared well able to maintain axonal conduction at 25 Hz, but without prior NMDA exposure axons stimulated at 25 Hz showed a functional decline of about 10% per min. Consistently, the decline of axonal conduction at increasing frequency of stimulation was even more aggravated when NMDA receptors had been blocked before by D-AP5 and 7CKA (Figure 4F). Taken together, these results strongly suggest that non-spiking axons lose oligodendroglial metabolic support over time.

In Vivo Relevance of Oligodendroglial NMDA Receptor Function

To confirm our key finding also in vivo, we focused on the spinal cord. Electrical stimulation of dorsal roots (L4) in anesthetized mice evoked stable CAPs that could be recorded from the dorsal columns (L1) (Figure 5A). We detected no overt differences between NR1 mutants and controls in spinal conduction properties or axon excitability (Figures 5B and 5C), confirming the overall integrity of myelinated tracts (Figures 5A, inset). Next, we monitored CAP (peak-to-peak) amplitudes following challenges at low (0.1 Hz), medium (10 Hz) and high frequency (100 Hz). At low or medium frequency (for 10 min), we observed no difference between mutants and controls (Figures 5D). However, upon high-frequency stimulation, CAP amplitudes dropped significantly faster in mutant mice (Figures 5E, inset left). When allowed to recover at low frequency (0.1 Hz), CAPs in mutant spinal cords recovered more slowly than in controls (Figures 5E, inset right).

Myelinated axons vary in length, diameter, and firing frequencies, suggesting that their long-term energy demands differ greatly (Perge et al., 2012). We anticipated that NR1 mutant mice with a developmentally reduced presence of GLUT1 in myelin sheaths develop at least some signs of axonal pathology. We therefore examined white matter integrity in different CNS regions of adult NR1 mutants and controls, kept under normal cage conditions (10–12 months) and without specific challenges. While most white and gray matter regions in mutant mice, including optic nerves, appeared devoid of pathology within the first year (data not shown), such changes became detectable in white matter tracts of the medulla (Figures 6A and S7A). In longitudinal sections, we observed an increased abundance of reactive microglia and astrogliosis (Figures 6A–6D). Also in spinal cord cross sections we occasionally noticed reactive microglia in white matter tracts of the dorsal and lateral columns (Figures S7B and S7C). By electron microscopy, we observed myelin delamination and degenerating axons in cervical spinal cord sections (Figures 6E and 6F) that were not a feature of wild-type mice.

The majority of myelinated axons in cortico-spinal tracts fire at a high frequency and comprise a high energy demanding white matter tract (Perge et al., 2012). We therefore performed a motor-behavioral analysis to assess the function of spinal tracts in adult NR1 mutant mice. Indeed, even on a simple rotarod test, 1 year old NR1 mutants revealed a significant deficit in performance when compared to age-matched controls (Figure 6G).

At the age of 19 months, NR1 mutants exhibited a severe neurological phenotype including hind limb clasping, hunchback, and ataxia (Figure 6H) caused by ongoing neurodegeneration, which became visible at 10 months. Signs of neuroinflammation and axonopathy were seen in all CNS white matter tracts (Figures 6I–6L).

DISCUSSION

Oligodendroglial metabolic support can explain why myelinated axons are vitally dependent on myelin integrity, independent of the myelin function in saltatory conduction (Griffiths et al., 1998; Kassmann et al., 2007; Lappe-Siefke et al., 2003). However, the question arises as to how glycolysis in oligodendrocytes is matched to different axonal energy needs and how excessive lactate production is avoided. Our study yields a novel working model in which oligodendrocytes regulate glucose utilization by using NMDA receptor signals as a surrogate marker for axonal spiking activity (Figure 7).

While NMDA receptors are widely studied in glutamatergic neurotransmission, the role of NMDA receptors in oligodendrocytes has remained enigmatic (De Biase et al., 2011; Guo et al., 2012; Káradóttir et al., 2005; Li et al., 2013; Lipton, 2006; Lundgaard et al., 2013; Micu et al., 2006; Piña-Crespo et al., 2010; Salter and Fern, 2005; Yang et al., 2014). In myelin, NR1 is associated with NR2C and NR3A subunits that provide a weak Mg^{2+} block (Burzomato et al., 2010; Das et al., 1998), suggesting that calcium entry does not require prior membrane depolarization. In development, NMDA receptors are most abundant in oligodendrocyte precursors (De Biase et al., 2010; Zhang et al., 2014). Unfortunately, the early functions of glutamate signaling were not revealed by the deletion of NR1 in OPC (De Biase et al., 2011; Guo et al., 2012). It is possible that calcium permeable AMPA receptors compensate functions other than GLUT1 trafficking, which is specifically regulated by NMDA receptor signaling. This is reminiscent of hippocampal LTP, which also requires NMDA receptors and is not compensated by AMPA receptors alone (Tsien et al., 1996).

Oligodendroglial NMDA receptors are localized in specialized microdomains of myelinating processes (Stirling and Stys, 2010; Stys, 2011) and also face the periaxonal space (Micu et al., 2006). Is NMDA receptor-dependent regulation of GLUT1 in oligodendrocytes and the non-compacted myelin compartment the same as GLUT4 regulation in other cell types (Bogan and Kandror, 2010)? In adipocytes, insulin-dependent GLUT4 trafficking requires calcium-dependent myosin motors (Yip et al., 2008). We were unable to mobilize GLUT1 with insulin in oligodendrocytes, but when triggered with NMDA, trafficking was expectedly calcium dependent and required a stable microtubule network (data not shown).

With the completion of developmental myelination, glycolysis products become gradually available to support the axonal energy metabolism, which is presumably more critical for fibers with high spiking activity. The ultrastructure of mature myelin is complex with narrow (non-compacted) cytosolic compartments in which glycolysis can take place. Once incorporated into these myelin membranes, glucose transporters are more likely to serve long-term functions than fast ("insulin-like") adaptations to changing energy needs. Indeed, our ex vivo experiment showed that it takes many hours for oligodendrocytes to metabolically respond to the loss of glutamate signaling. However, activity-dependent

regulation of axonal energy metabolism may be clinically relevant, e.g., in the aging brain or in neurodegenerative diseases ("use it or lose it").

It is therefore of interest that NR1 mutant mice, when kept in standard housing (i.e., without physical challenges), showed signs of neurodegeneration beginning in the medulla and spinal cord at 10 months of age and progressing later to all CNS white matter tracts. Here, visible axonopathy and inflammation are most likely a "tip of the iceberg," reflecting reduced energy metabolism in (many more) myelinated axons in vivo.

Finally, we note that astrocytes can also support axon function by releasing lactate in the white matter. They have direct access to the vasculature, store glycogen, and rapidly respond to energy deprivation with glycogen breakdown (Brown and Ransom, 2007). Theoretically, astrocytes may compensate some metabolic functions in oligodendroglial NMDA receptor mutants. The regulated metabolic interactions between axons, oligodendrocytes, and astrocytes are increasingly recognized as key for normal white matter function and likely for axon survival in many neurodegenerative diseases.

EXPERIMENTAL PROCEDURES

Mouse Strains

Female *Cnp1*-Cre mice (RRID: MGI_3051754) (Lappe-Siefke et al., 2003) were crossbred to floxed NR1 (gene symbol *Grin1*) mice (RRID: MGI_2175051) (Tsien et al., 1996). Conditional knockout animals were $Grin1^{flox/flox*}Cnp1^{Cre/+}$ mice. As controls, we used $Cnp1^{Cre/+}$, $Grin1^{flox/flox*}Cnp1^{+/+}$, or $Grin1^{flox/+*}Cnp1^{Cre/+}$ mice obtained as respective littermates. Some of the mice also carried the R26-stop-EYFP reporter gene for Cre activity (RRID: IMSR_JAX:006148) (Srinivas et al., 2001). Mice were maintained on the C57Bl6 background. Experiments were carried out mainly on male mice. Animal experiments were performed according to German, Spanish, and European guide lines for Animal Experimentation.

Cell Culture Preparation

Primary mouse or rat oligodendrocyte progenitor cells (OPCs) were isolated from cerebral cortices at P0–P2 as described previously (Barros et al., 2009; McCarthy and de Vellis, 1980). Cells were grown in DMEM (Lonza) supplemented with 10% fetal calf serum, Glutamax (Invitrogen), Penicillin and Streptomycin (Invitrogen) at 37°C, and 5% CO_2. Following OPC isolation, cells were differentiated for 5 days in Sato's medium. For all experiments, Glutamax was withdrawn from the growth medium in the last 12–16 hr of differentiation. OPCs utilized for biotinylation assays, 2-deoxyglucose uptake, or lactate release were further purified to 98.2% ± 0.3% by negative selection immunopanning (Barres et al., 1992).

Immunocytochemistry

For GLUT1 and MCT1 immunocytochemistry, differentiated cells were treated for 30 min at 37°C with 100 μM NMDA. Glycine as co-agonist for NMDA receptors was already present in the medium. NMDA receptor blockers D-AP5 and/or 7CKA (100 μM) were

applied 30 min prior to NMDA stimulation. Plasma membranes of mature oligodendrocytes were labeled with anti-galactocerebroside (GalC) antibody (Millipore Cat# MAB342 RRID: AB_94857) for 15 min at 37°C prior to fixation with 4% paraformaldehyde for 10 min at RT. Cells were permeabilized with ice-cold methanol for 5 min, washed with PBS, and incubated with anti-GLUT1 antibody (Abcam Cat# ab32551 RRID: AB_732605) or with anti-MCT1 (Millipore Cat# AB1286 RRID: AB_90565) overnight at 4°C. Analysis was carried out on confocal stacks of individual cells using ImageJ (http://rsb.info.nih.gov/ij/). Data are presented as the ratio of GLUT1 or MCT1 signal area to GalC area. Three individual experiments with 14–24 cells per condition were analyzed. Data were grouped per experiment and normalized to control condition.

Cell Surface Biotinylation

Immunopanned oligodendrocytes were treated with NMDA receptor agonists or antagonists as described above. Cell surface-associated proteins were labeled by incubation with 0.5 mg/ml membrane-impermeable EZ-link Sulfo-NHS-Biotin (Thermo Scientific) at 4°C for 30 min. After removing unbound biotin, cells were lysed for 15 min on ice with 1% Triton X-100, 0.2% SDS in PBS (pH 7.4) containing protease/phosphatase inhibitors. To isolate biotinylated proteins, 350–450 μg of lysate was incubated overnight at 4°C with 150 μl of 50% Pierce Streptavidin Agarose Resin in PBS (pH 7.2). After elution of biotinylated material, proteins were resolved by SDS-PAGE and immunoblotted with anti-GLUT1 or anti-MCT1 antibodies as described below.

Glucose Sensor Imaging

Rat mixed glial cells (after 8–12 days in culture) were transfected (using Fugene HD, Roche) with glucose sensor FLII12Pglu-700μ 6 (Takanaga et al., 2008; Addgene plasmid 17866). 1 day after transfection, OPCs were isolated and further cultivated for 5 days. For details on FRET imaging, see Supplemental Information. NMDA receptor agonists and antagonists (each 100 μM) were applied, and FRET changes were analyzed. For control experiments and sensor calibration (Bittner et al., 2010), cells were incubated without glucose or adding either iodoacetate (glycolysis inhibitor, 1 mM) or cytochalasin B (glucose transporter blocker, 40 μM).

2-Deoxyglucose Uptake Measurements

Immunopanned oligodendrocytes differentiated for 5 days were incubated for 25 min in the presence or absence of NMDA/Gly (100 μM) in a modified medium (in mM: NaCl 91.17; KCl 5.37; NaH_2PO_4 0.91; Na_2HPO_4 0.23; $NaHCO_3$ 17.86; $MgSO_4$ 0.81; $CaCl_2$ 1.8; NaOH 16.7; HEPES 20; glucose 10; adjusted to pH 7.4 with HCl after equilibration with 5% CO2). Then glucose was replaced by 10 mM 2-deoxyglucose (2DG) for 5 min. 2-deoxyglucose-6-phosphate present within the cells was quantified using a commercial kit according to the instructions of the manufacturer (Cosmobio).

Measurements of Lactate Release by NMR

Immunopanned oligodendrocytes were differentiated for 4 days in Sato's medium containing 25 mM unlabeled glucose and for an additional day in Sato's medium

containing 25 mM U-^{13}C$_6$-glucose. 100 μM NMDA/Gly was added for 30 min at 37°C in modified medium (see above) containing U-^{13}C$_6$-glucose. Conditioned media was immediately collected and snap frozen until NMR analysis. For details on NMR analysis, see Supplemental Information.

Immunohistochemistry

For NR1 labeling, mice were perfused with ice-cold artificial cerebrospinal fluid (ACSF). Optic nerves were isolated and immersion fixed with 4% PFA for 2 hr at RT and prepared for later cryo-sectioning. Slide-mounted sections (12 μm) were air-dried at RT and then treated with 0.3% Triton X-100 and 5% horse serum for 1 hr. Primary antibodies for NR1 (1:250, Millipore Cat# MAB363, RRID: AB_94946) and MBP (1:300, rabbit, Dako) were incubated overnight at 4°C in the same solution. Secondary antibodies were incubated in 2% horse serum for 2 hr at RT.

For analysis of local inflammation and pathology, paraffin sections of perfusion-fixed tissues were used. Sections were treated with primary antibodies diluted in PBS/BSA (1% w/v BSA) overnight at 4°C. Dilutions were as follows: GFAP (1:200, mouse, Novocastra), Mac3 (1:400, rat, BD PharMingen), and APP (1:1000, Millipore Cat# MAB348 RRID: AB_94882). Biotinylated secondary antibodies were then incubated for 30 min at RT, and chromogenic staining was completed using HRP-DAB detection.

Protein Analysis

Protein lysates of optic nerves from individual mice were prepared using the Precellys Ceramic Kit 1.4 mm and the Precellys 24 homogenizer (Peqlab). Nerves were homogenized in 150 μl sucrose buffer (in mM: 320 sucrose, 10 Tris [pH 7.4], 1 NaHCO$_3$, and 1 MgCl$_2$) and protease inhibitors (Complete tablets, Roche). For Western blotting, 30 μg protein lysate was size-separated on 12% SDS-polyacrylamide gels and blotted onto nitrocellulose membranes following instructions from BioRad. Primary antibodies to NR1 (1:500, Millipore Cat# MAB363, RRID: AB_94946) and GAPDH (1:2000, Enzo Life Sciences Cat# ADI-CSA-335-E, RRID: AB_2039148) were diluted in blocking buffer (5% milk) and incubated overnight at 4°C. Membranes were washed in 0.05% Tween prepared in phosphate buffer (PBS-T) followed by incubation with a horseradish peroxidase-conjugated secondary antibody. Proteins were detected with an enhanced chemiluminescence kit (Western Lightning, PerkinElmer) according to the manufacturer's instructions. Exposed ECL films (Amersham Biosciences) were scanned at grayscale (300 dpi resolution) using a regular image scanner, followed by densitometric analysis with ImageJ. The peak intensity for NR1 was normalized to the peak intensity of GAPDH.

Immunoelectron Microscopy

Freshly dissected optic nerves were immersion fixed with 4% formaldehyde and 0.2% glutaraldehyde in 0.1 M phosphate buffer containing 0.5% NaCl. After embedding in 10% gelatine and subsequent infiltration with 2.3 M sucrose in 0.1 M PB overnight, small blocks of gelatin containing optic nerve pieces were mounted onto aluminum pins for ultramicrotomy and frozen in liquid nitrogen. Ultrathin cryosections were picked up with a 1:1 mixture of 2% methylcellulose and 2.3 M sucrose. Sections were incubated

with antibodies against GLUT1 (1:100, Abcam Cat# ab32551 RRID: AB_732605) and MCT1 (1:1,000, Millipore Cat# AB1286 RRID: AB_90565) and detected with protein A-gold (10 nm, obtained from the Cell Microscopy Center, Department of Cell Biology, University Medical Center Utrecht, NL), and by anti-chicken immunogold (10 nm, Aurion), respectively. Sections were analyzed with a LEO EM912AB (Zeiss), and digital micrographs were obtained with an on-axis 2048×2048-CCD camera (TRS, Moorenweis). For quantification, 10–12 randomly taken images from three controls and three NR1 mutants were assessed. Per image, all myelinated axons and immunogold particles associated with myelinated axons were counted, and a ratio of immunogold particles to the number of myelinated axons was calculated. The mean ratio per animal was then normalized to controls.

Myelin Preparation and Immunoblotting

Myelin was purified as described before (Norton and Poduslo, 1973) from mouse brain homogenate in 0.32 M sucrose. Immunoblotting was performed as described before (Werner et al., 2007). Briefly, 30 μg of protein were separated on 10% SDS-polyacrylamide gels, blotted onto polyvinylidene difluoride membranes (Roche), and incubated with primary antibodies for GLUT1 (1:500, Abcam Cat# ab32551 RRID: AB_732605), MCT1 (1:1,000, Millipore Cat# AB1286 RRID: AB_90565), and SIRT2 (1:2,000) (Dryden et al., 2003). Blots were incubated with horseradish peroxidase-coupled secondary antibodies (Dianova) and developed by enhanced chemiluminescence (Western Lightning ECL, PerkinElmer) using a luminescence imager (Intas).

Electron Microscopy and Morphometry

Optic nerves were acutely removed and either immersion-fixed for conventional sample preparation or cryofixed by HPF and freeze substituted as described in detail (Möbius et al., 2010). For analysis of axonal pathology, animals were perfusion-fixed (4% formaldehyde, 2.5% glutaraldehyde). For structural analysis of optic nerves that were subjected to OGD, nerves were directly immersion-fixed (4% formaldehyde, 2.5% glutaraldehyde). For analysis of unmyelinated, myelinated, and ensheathed axons (defined as 1–3 uncompacted layers), 4–6 EM images with $12,000\times$ magnification 400–700 axons were counted for each nerve. Data were grouped per animal. For g-ratio analysis, 4–5 random overview pictures were taken at $8,000\times$ magnification, 200 axons analyzed using ImageJ (images were blinded for experimenter). G-ratios (axonal diameter divided by the fiber diameter including the myelin sheath) were calculated from circular areas equivalent to the measured areas of axons and myelin sheath including the axon.

Optic Nerve Recordings

Following anesthesia and decapitation, nerves were gently removed, placed into an interface perfusion chamber (Haas Top, Harvard Apparatus), and superfused with ACSF containing the following (in mM): 124 NaCl, 3.0 KCl, 2.0 $CaCl_2$, 2.0 $MgSO_4$, 1.25 NaH_2PO_4, 23 $NaHCO_3$, and 10 glucose. Perfusion chamber was continuously aerated by a humidified gas mixture of 95% O_2/5% CO_2, and experiments were performed at 37°C.

For oxygen-glucose deprivation (OGD), the protocol was performed as described previously (Baltan et al., 2008). CAPs were elicited every 30 s, and OGD (applied for 60 min) was induced by switching to glucose-free ACSF and a gas mixture containing 95% N_2/5% CO_2. After OGD control ACSF and O_2 were restored and CAPs were recorded for up to 2–3 hr, responses were stabilized within 20 to 30 min. When L-Lactate (20 mM, Sigma) was used during recovery, it was substituted for 20 mM NaCl.

CAP area is proportional to the total number of excited axons (Stys et al., 1991). Irreversible injury was measured by determining residual CAP area 1.5–2 hr after conclusion of OGD, normalized to baseline CAP area.

For the long-term ex vivo analysis, wild-type nerves were continuously superfused with ACSF containing either NMDA and glycine (NMDA/Gly 100 μM), NMDA/Gly plus 7CKA and D-AP5 (7CKA/D-AP5 100 μM), or DMSO only (DMSO Control). After 16 hr of treatment, CAPs were recorded at 0.2 Hz to obtain baseline, and then nerves were challenged with a gradual increase in stimulation frequency (from 1 to 100 Hz), with each stimulus train lasting 30 s. For 1 and 5 Hz stimulations, CAPs were continuously recorded. For 10, 25, 50, and 100 Hz stimulations, CAPs were sampled after a burst of each 100 stimuli with an inter-burst interval of 300 ms. CAP area of the graded responses were analyzed for each treatment group (2.1 ms after stimulus onset) and normalized to baseline.

In Vivo Spinal Cord CAP Recordings

For details, see Supplemental Information. Stimulation and recording from spinal cord axons in vivo were performed with bipolar platinum electrodes. Square-wave constant voltage pulses (100 μs) were used to stimulate the dorsal root L4, and CAPs were recorded from the ipsilateral fasciculus gracilis at spinal cord level L1. Dorsal roots were stimulated at different frequencies (0.1, 10, and 100 Hz), and CAP recordings were sampled at 50 kHz. Distance between the electrodes was measured using a thin cotton thread to evaluate conduction velocities. For analysis of axonal firing strength, the peak-to-peak amplitude (of the first and most robust peak of the CAP recording) was monitored over time and normalized to baseline (0.1 Hz).

Rotarod and Clinical Score

Mice (10–12 months) were placed on a horizontal rod at 1 rpm and accelerated with 1 rpm every 10 s (three tests per trial). The clinical scores at the age of 19 months were as follows: 0, asymptomatic; 1, hind limb clasping; 2, additionally, hunchback visible; 3, additionally, slipping during walking on a grid; 3.5, additionally, not able to hold on an inverted grid; 4, additionally, hind limb ataxia, not able to hold on an upright grid and reduced righting reflex; 4.5, spastic hind limbs.

Statistical Analysis

Inter-group comparisons were done by Mann Whitney t test or two-tailed Student's t test. For multiple comparisons, data were analyzed with one-way or two-way ANOVA with Bonferroni's post-test or using linear mixed effects models (lme4 package v.1.1.9; https://cran.r-project.org/web/packages/lme4/). All analyses were conducted through GraphPad

Prism 4 or R (v.3.2.2, R Core Team, 2015). The levels of significance were set as *p < 0.05; **p < 0.01; ***p < 0.001. Data are represented as means ± SEM.

Supplementary Material

Refer to Web version on PubMed Central for supplementary material.

REFERENCES

Baltan S, Besancon EF, Mbow B, Ye Z, Hamner MA, and Ransom BR (2008). White matter vulnerability to ischemic injury increases with age because of enhanced excitotoxicity. J. Neurosci. 28, 1479–1489. [PubMed: 18256269]

Barres BA, Hart IK, Coles HS, Burne JF, Voyvodic JT, Richardson WD, and Raff MC (1992). Cell death and control of cell survival in the oligodendrocyte lineage. Cell 70, 31–46. [PubMed: 1623522]

Barros CS, Nguyen T, Spencer KS, Nishiyama A, Colognato H, and Müller U (2009). Beta1 integrins are required for normal CNS myelination and promote AKT-dependent myelin outgrowth. Development 136, 2717–2724. [PubMed: 19633169]

Barry JM (2015). Axonal activity in vivo: technical considerations and implications for the exploration of neural circuits in freely moving animals. Front. Neurosci. 9, 153. [PubMed: 25999806]

Bittner CX, Loaiza A, Ruminot I, Larenas V, Sotelo-Hitschfeld T, Gutiérrez R, Córdova A, Valdebenito R, Frommer WB, and Barros LF (2010). High resolution measurement of the glycolytic rate. Front. Neuroenergetics 2, 2. [PubMed: 20725519]

Bogan JS, and Kandror KV (2010). Biogenesis and regulation of insulin-responsive vesicles containing GLUT4. Curr. Opin. Cell Biol. 22, 506–512. [PubMed: 20417083]

Brown AM, and Ransom BR (2007). Astrocyte glycogen and brain energy metabolism. Glia 55, 1263–1271. [PubMed: 17659525]

Burzomato V, Frugier G, Pérez-Otaño I, Kittler JT, and Attwell D (2010). The receptor subunits generating NMDA receptor mediated currents in oligodendrocytes. J. Physiol. 588, 3403–3414. [PubMed: 20660562]

Das S, Sasaki YF, Rothe T, Premkumar LS, Takasu M, Crandall JE, Dikkes P, Conner DA, Rayudu PV, Cheung W, et al. (1998). Increased NMDA current and spine density in mice lacking the NMDA receptor subunit NR3A. Nature 393, 377–381. [PubMed: 9620802]

De Biase LM, Nishiyama A, and Bergles DE (2010). Excitability and synaptic communication within the oligodendrocyte lineage. J. Neurosci. 30, 3600–3611. [PubMed: 20219994]

De Biase LM, Kang SH, Baxi EG, Fukaya M, Pucak ML, Mishina M, Calabresi PA, and Bergles DE (2011). NMDA receptor signaling in oligodendrocyte progenitors is not required for oligodendrogenesis and myelination. J. Neurosci. 31, 12650–12662. [PubMed: 21880926]

Dryden SC, Nahhas FA, Nowak JE, Goustin AS, and Tainsky MA (2003). Role for human SIRT2 NAD-dependent deacetylase activity in control of mitotic exit in the cell cycle. Mol. Cell. Biol. 23, 3173–3185. [PubMed: 12697818]

Emery B (2010). Regulation of oligodendrocyte differentiation and myelination. Science 330, 779–782. [PubMed: 21051629]

Ferreira JM, Burnett AL, and Rameau GA (2011). Activity-dependent regulation of surface glucose transporter-3. J. Neurosci. 31, 1991–1999. [PubMed: 21307237]

Fünfschilling U, Supplie LM, Mahad D, Boretius S, Saab AS, Edgar J, Brinkmann BG, Kassmann CM, Tzvetanova ID, Möbius W, et al. (2012). Glycolytic oligodendrocytes maintain myelin and long-term axonal integrity. Nature 485, 517–521. [PubMed: 22622581]

Gibson EM, Purger D, Mount CW, Goldstein AK, Lin GL, Wood LS, Inema I, Miller SE, Bieri G, Zuchero JB, et al. (2014). Neuronal activity promotes oligodendrogenesis and adaptive myelination in the mammalian brain. Science 344, 1252304. [PubMed: 24727982]

Griffiths I, Klugmann M, Anderson T, Yool D, Thomson C, Schwab MH, Schneider A, Zimmermann F, McCulloch M, Nadon N, and Nave KA (1998). Axonal swellings and degeneration in mice lacking the major proteolipid myelin. Science 280, 1610–1613. [PubMed: 9616125]

Guo F, Maeda Y, Ko EM, Delgado M, Horiuchi M, Soulika A, Miers L, Burns T, Itoh T, Shen H, et al. (2012). Disruption of NMDA receptors in oligodendroglial lineage cells does not alter their susceptibility to experimental autoimmune encephalomyelitis or their normal development. J. Neurosci. 32, 639–645. [PubMed: 22238099]

Hamilton NB, Kolodziejczyk K, Kougioumtzidou E, and Attwell D (2016). Proton-gated Ca(2+)-permeable TRP channels damage myelin in conditions mimicking ischaemia. Nature 529, 523–527. [PubMed: 26760212]

Hildebrand C, and Waxman SG (1984). Postnatal differentiation of rat optic nerve fibers: electron microscopic observations on the development of nodes of Ranvier and axoglial relations. J. Comp. Neurol. 224, 25–37. [PubMed: 6715578]

Káradóttir R, Cavelier P, Bergersen LH, and Attwell D (2005). NMDA receptors are expressed in oligodendrocytes and activated in ischaemia. Nature 438, 1162–1166. [PubMed: 16372011]

Kassmann CM, Lappe-Siefke C, Baes M, Brügger B, Mildner A, Werner HB, Natt O, Michaelis T, Prinz M, Frahm J, and Nave KA (2007). Axonal loss and neuroinflammation caused by peroxisome-deficient oligodendrocytes. Nat. Genet. 39, 969–976. [PubMed: 17643102]

Kukley M, Capetillo-Zarate E, and Dietrich D (2007). Vesicular glutamate release from axons in white matter. Nat. Neurosci. 10, 311–320. [PubMed: 17293860]

Lappe-Siefke C, Goebbels S, Gravel M, Nicksch E, Lee J, Braun PE, Griffiths IR, and Nave KA (2003). Disruption of Cnp1 uncouples oligodendroglial functions in axonal support and myelination. Nat. Genet. 33, 366–374. [PubMed: 12590258]

Lee Y, Morrison BM, Li Y, Lengacher S, Farah MH, Hoffman PN, Liu Y, Tsingalia A, Jin L, Zhang PW, et al. (2012). Oligodendroglia metabolically support axons and contribute to neurodegeneration. Nature 487, 443–448. [PubMed: 22801498]

Li C, Xiao L, Liu X, Yang W, Shen W, Hu C, Yang G, and He C (2013). A functional role of NMDA receptor in regulating the differentiation of oligodendrocyte precursor cells and remyelination. Glia 61, 732–749. [PubMed: 23440860]

Lipton SA (2006). NMDA receptors, glial cells, and clinical medicine. Neuron 50, 9–11. [PubMed: 16600850]

Liu J, Dietz K, DeLoyht JM, Pedre X, Kelkar D, Kaur J, Vialou V, Lobo MK, Dietz DM, Nestler EJ, et al. (2012). Impaired adult myelination in the prefrontal cortex of socially isolated mice. Nat. Neurosci. 15, 1621–1623. [PubMed: 23143512]

Lundgaard I, Luzhynskaya A, Stockley JH, Wang Z, Evans KA, Swire M, Volbracht K, Gautier HO, Franklin RJ, Attwell D, and Káradóttir RT; Charles Ffrench-Constant (2013). Neuregulin and BDNF induce a switch to NMDA receptor-dependent myelination by oligodendrocytes. PLoS Biol. 11, e1001743. [PubMed: 24391468]

Matute C (2010). Calcium dyshomeostasis in white matter pathology. Cell Calcium 47, 150–157. [PubMed: 20036774]

McCarthy KD, and de Vellis J (1980). Preparation of separate astroglial and oligodendroglial cell cultures from rat cerebral tissue. J. Cell Biol. 85, 890–902. [PubMed: 6248568]

Micu I, Jiang Q, Coderre E, Ridsdale A, Zhang L, Woulfe J, Yin X, Trapp BD, McRory JE, Rehak R, et al. (2006). NMDA receptors mediate calcium accumulation in myelin during chemical ischaemia. Nature 439, 988–992. [PubMed: 16372019]

Micu I, Plemel JR, Lachance C, Proft J, Jansen AJ, Cummins K, van Minnen J, and Stys PK (2016). The molecular physiology of the axo-myelinic synapse. Exp. Neurol. 276, 41–50. [PubMed: 26515690]

Miller RH, David S, Patel R, Abney ER, and Raff MC (1985). A quantitative immunohistochemical study of macroglial cell development in the rat optic nerve: in vivo evidence for two distinct astrocyte lineages. Dev. Biol. 111, 35–41. [PubMed: 3896893]

Möbius W, Cooper B, Kaufmann WA, Imig C, Ruhwedel T, Snaidero N, Saab AS, and Varoqueaux F (2010). Electron microscopy of the mouse central nervous system. Methods Cell Biol. 96, 475–512. [PubMed: 20869535]

Morrison BM, Lee Y, and Rothstein JD (2013). Oligodendroglia: metabolic supporters of axons. Trends Cell Biol. 23, 644–651. [PubMed: 23988427]

Nave KA (2010). Myelination and the trophic support of long axons. Nat. Rev. Neurosci. 11, 275–283. [PubMed: 20216548]

Nave KA, and Werner HB (2014). Myelination of the nervous system: mechanisms and functions. Annu. Rev. Cell Dev. Biol. 30, 503–533. [PubMed: 25288117]

Norton WT, and Poduslo SE (1973). Myelination in rat brain: method of myelin isolation. J. Neurochem. 21, 749–757. [PubMed: 4271082]

Perge JA, Niven JE, Mugnaini E, Balasubramanian V, and Sterling P (2012). Why do axons differ in caliber? J. Neurosci. 32, 626–638. [PubMed: 22238098]

Piña-Crespo JC, Talantova M, Micu I, States B, Chen HS, Tu S, Nakanishi N, Tong G, Zhang D, Heinemann SF, et al. (2010). Excitatory glycine responses of CNS myelin mediated by NR1/NR3 "NMDA" receptor subunits. J. Neurosci. 30, 11501–11505. [PubMed: 20739572]

Rinholm JE, Hamilton NB, Kessaris N, Richardson WD, Bergersen LH, and Attwell D (2011). Regulation of oligodendrocyte development and myelination by glucose and lactate. J. Neurosci. 31, 538–548. [PubMed: 21228163]

Saab AS, Tzvetanova ID, and Nave KA (2013). The role of myelin and oligodendrocytes in axonal energy metabolism. Curr. Opin. Neurobiol. 23, 1065–1072. [PubMed: 24094633]

Salter MG, and Fern R (2005). NMDA receptors are expressed in developing oligodendrocyte processes and mediate injury. Nature 438, 1167–1171. [PubMed: 16372012]

Snaidero N, Möbius W, Czopka T, Hekking LH, Mathisen C, Verkleij D, Goebbels S, Edgar J, Merkler D, Lyons DA, et al. (2014). Myelin membrane wrapping of CNS axons by PI(3,4,5)P3-dependent polarized growth at the inner tongue. Cell 156, 277–290. [PubMed: 24439382]

Srinivas S, Watanabe T, Lin CS, William CM, Tanabe Y, Jessell TM, and Costantini F (2001). Cre reporter strains produced by targeted insertion of EYFP and ECFP into the ROSA26 locus. BMC Dev. Biol. 1, 4. [PubMed: 11299042]

Stirling DP, and Stys PK (2010). Mechanisms of axonal injury: internodal nanocomplexes and calcium deregulation. Trends Mol. Med. 16, 160–170. [PubMed: 20207196]

Stys PK (2011). The axo-myelinic synapse. Trends Neurosci. 34, 393–400. [PubMed: 21741098]

Stys PK, Ransom BR, and Waxman SG (1991). Compound action potential of nerve recorded by suction electrode: a theoretical and experimental analysis. Brain Res. 546, 18–32. [PubMed: 1855148]

Takanaga H, Chaudhuri B, and Frommer WB (2008). GLUT1 and GLUT9 as major contributors to glucose influx in HepG2 cells identified by a high sensitivity intramolecular FRET glucose sensor. Biochim. Biophys. Acta 1778, 1091–1099. [PubMed: 18177733]

Tekkök SB, Brown AM, Westenbroek R, Pellerin L, and Ransom BR (2005). Transfer of glycogen-derived lactate from astrocytes to axons via specific monocarboxylate transporters supports mouse optic nerve activity. J. Neurosci. Res. 81, 644–652. [PubMed: 16015619]

Tekkök SB, Ye Z, and Ransom BR (2007). Excitotoxic mechanisms of ischemic injury in myelinated white matter. J. Cereb. Blood Flow Metab. 27, 1540–1552. [PubMed: 17299453]

Tsien JZ, Huerta PT, and Tonegawa S (1996). The essential role of hippocampal CA1 NMDA receptor-dependent synaptic plasticity in spatial memory. Cell 87, 1327–1338. [PubMed: 8980238]

Wake H, Lee PR, and Fields RD (2011). Control of local protein synthesis and initial events in myelination by action potentials. Science 333, 1647–1651. [PubMed: 21817014]

Werner HB, Kuhlmann K, Shen S, Uecker M, Schardt A, Dimova K, Orfaniotou F, Dhaunchak A, Brinkmann BG, Möbius W, et al. (2007). Proteolipid protein is required for transport of sirtuin 2 into CNS myelin. J. Neurosci. 27, 7717–7730. [PubMed: 17634366]

Wyss MT, Jolivet R, Buck A, Magistretti PJ, and Weber B (2011). In vivo evidence for lactate as a neuronal energy source. J. Neurosci. 31, 7477–7485. [PubMed: 21593331]

Yang X, Hamner MA, Brown AM, Evans RD, Ye ZC, Chen S, and Ransom BR (2014). Novel hypoglycemic injury mechanism: N-methyl-D-aspartate receptor-mediated white matter damage. Ann. Neurol. 75, 492–507. [PubMed: 24242287]

Yip MF, Ramm G, Larance M, Hoehn KL, Wagner MC, Guilhaus M, and James DE (2008). CaMKII-mediated phosphorylation of the myosin motor Myo1c is required for insulin-stimulated GLUT4 translocation in adipocytes. Cell Metab. 8, 384–398. [PubMed: 19046570]

Zhang Y, Chen K, Sloan SA, Bennett ML, Scholze AR, O'Keeffe S, Phatnani HP, Guarnieri P, Caneda C, Ruderisch N, et al. (2014). An RNA-sequencing transcriptome and splicing database of glia, neurons, and vascular cells of the cerebral cortex. J. Neurosci. 34, 11929–11947. [PubMed: 25186741]

Ziskin JL, Nishiyama A, Rubio M, Fukaya M, and Bergles DE (2007). Vesicular release of glutamate from unmyelinated axons in white matter. Nat. Neurosci. 10, 321–330. [PubMed: 17293857]

Highlights

- Oligodendroglial NMDA receptors regulate GLUT1 trafficking and glucose import

- Mouse mutants lacking NMDA receptors from oligodendrocytes are delayed in myelination

- Activation of oligodendroglial NMDA receptor supports the axonal energy metabolism

- Mice lacking oligodendroglial NMDA receptors develop late-onset axonopathy and neuroinflammation
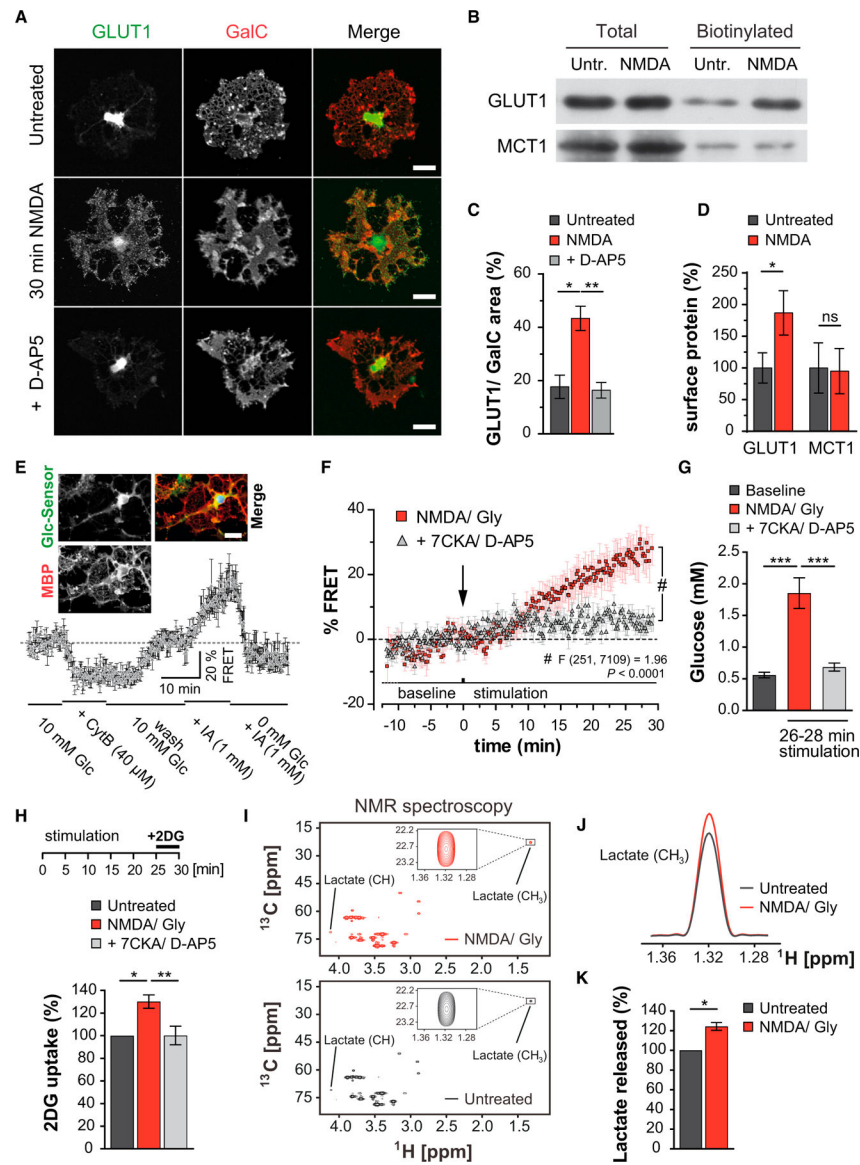
Figure 1. NMDA Stimulates GLUT1 Surface Expression and Glucose Uptake by Cultured Oligodendrocytes

(A) Oligodendrocyte immunostained for GLUT1 and GalC. NMDA receptor stimulation mobilizes GLUT1 and increases its cell surface expression, which is blocked by D-AP5. Scale bar, 20 μm.

(B) GLUT1 and MCT1 immunoblots following cell surface biotinylation of immunopanned NMDA-treated oligodendrocytes and controls.

(C) Quantification of the experiments giving the ratio of GLUT1:GalC in a stained area of n = 3 experiments and 20–24 cells per condition (*p < 0.05, **p < 0.01 one-way ANOVA with Bonferroni's multiple comparisons test).

(D) Quantification of the experiments in (B), normalizing biotinylated to total protein (p = 0.03, n = 3; paired t test). MCT1 surface expression is unchanged.

(E) FRET imaging of oligodendrocytes expressing a glucose sensor (Takanaga et al., 2008) (FLII12Pglu-700μ 6). Intracellular glucose levels (normalized to baseline FRET

signals, n = 4) drop with addition of cytochalasin B (CytB, glucose transporter blocker) or increase with iodoacetate (IA, glycolysis inhibitor). Note that intracellular glucose is rapidly phosphorylated and undetectable.

Inset: oligodendrocyte transfected with the glucose sensor and counterstained for MBP. Note that the sensor is mainly located in the soma and main processes. Scale bar, 20 μm.

(F) NMDA receptor stimulation (by applying 100 μM NMDA and glycine) increases FRET signals that can be blocked by the addition of 7CKA and D-AP5 ($F_{interaction}$(251, 7,109) = 1.96, p < 0.0001, two-way ANOVA).

(G) Quantification of calibrated FRET signals of NMDA-stimulated oligodendrocytes (26–28 min), compared to baseline and cells also receiving 7CKA and D-AP5 (***p < 0.001, one way ANOVA with Bonferroni's multiple comparisons test).

(H) Immunopanned oligodendrocytes stimulated with NMDA/Gly (25 min) before switching to 2-deoxyglucose (2DG, 10 mM, 5 min). Increased 2DG uptake was blocked by 7CKA and D-AP5 (n = 5 experiments, *p < 0.05, **p < 0.01; paired t test).

(I) ^{13}C, ^{1}H-HSQC spectra at 700 MHz corresponding to proton resonance from the culture medium of immunopanned oligodendrocytes 30 min after exposure to NMDA/Gly (top) and controls (bottom). Boxed: lactate signals. Quantification by comparison of the peak volume of lactate methyl group to the internal standard DSS.

(J) Increased lactate following NMDA/Gly treatment, depicted by overlaying the 1D-^{1}H slices of spectra in the lactate methyl signal range.

(K) Lactate release after NMDA receptor stimulation increased to 124% ± 4% (n = 4 paired NMR experiments, p = 0.023 paired t test).
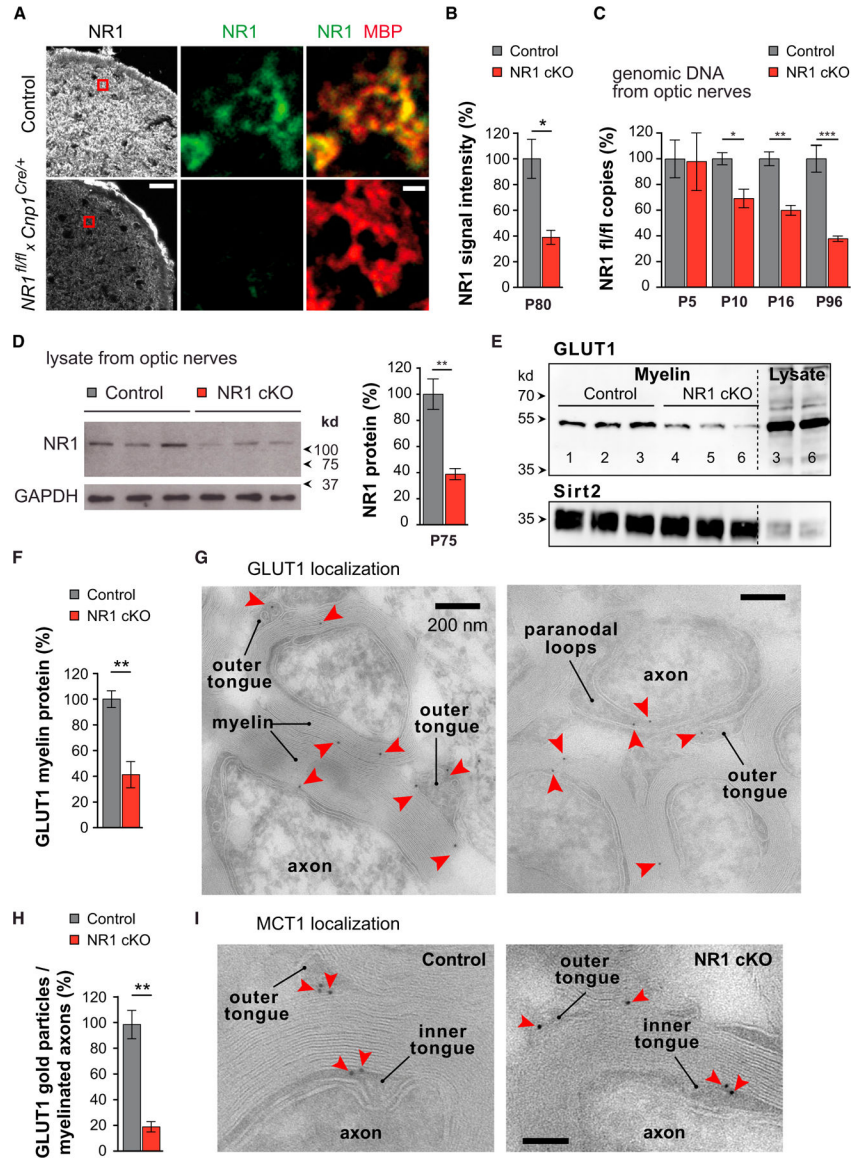
Figure 2. Oligodendroglial NMDA Receptor Mutants with Reduced GLUT1 Incorporation into Myelin

(A) Immunostaining of NR1 in optic nerve cross sections at age P80 from control and NR1 cKO mice (left panel). Higher magnifications (middle and right panels) reveal that NR1 (green) is absent from mutants and overlaps with MBP (red) in control mice. Scale bars, 20 μm (left) and 1 μm. See also Figure S2A.

(B) Quantitation of NR1 staining intensity from whole optic nerve sections (n = 3; p = 0.019, Student's t test).

(C) Cre-mediated recombination of genomic DNA in individual optic nerves of each genotype as quantified by qPCR. Depicted is the relative abundance of the floxed NR1 allele after recombination (normalized to the abundance in NR1^fl/fl littermate controls, defined as 100% at different ages). In NR1 mutant nerves, the abundance of NR1 flox copies was determined at ages P5 (98% ± 22% flox copies remaining; n = 5 versus 4, p = 0.939), age

P10 (69% ± 7%; n = 4, p = 0.0119), age P16 (60% ± 4%; n = 4 versus 3, p = 0.0024), and P96 (38% ± 2%; n = 4 versus 9, p < 0.0001).

(D) Western blot analysis of NR1 expression in individual nerves from mutant and control mice at age P75. Quantification revealed a reduction by 61% ± 12% in NR1 cKO nerves (n = 3, p = 0.0079). GAPDH, loading control.

(E) By western blotting, GLUT1 is reduced in purified myelin of NR1 mutants (Sirt2, loading control).

(F) Quantification of E (n = 3; p = 0.008, Student's t test).

(G) Localization of GLUT1 by immunogold labeling. In optic nerve cross sections, GLUT1 was detected in myelin sheaths, the outer tongue, and paranodal loops. Scale bar, 200 nm. Gold particles, red arrows.

(H) Reduced abundance of immunogold labeled GLUT1 in myelin of NR1 mutant optic nerves when compared to littermate controls (10–12 randomly taken images per animal, n = 3; p = 0.0025, Student's t test).

(I) By immunogold labeling, MCT1 is associated with adaxonal (outer tongue) and abaxonal (inner tongue) myelinic channels, without difference between mutants and controls. Scale bar, 100 nm.
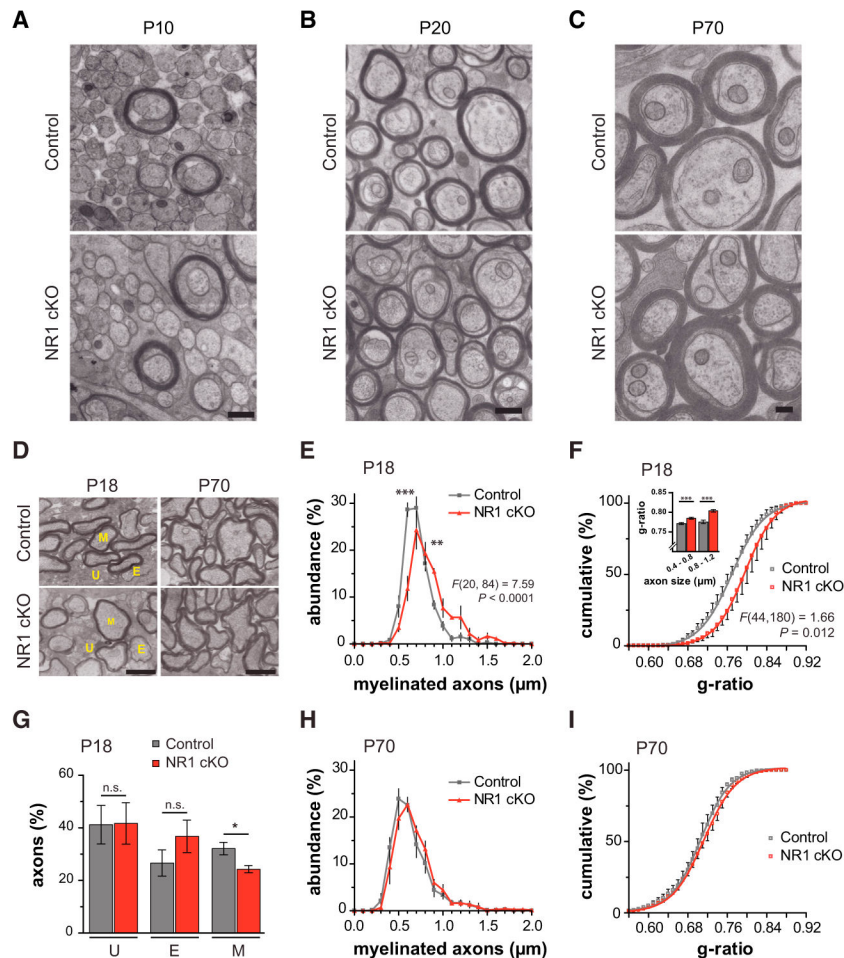
Figure 3. Myelination in the Absence of Oligodendroglial NMDA Receptors In Vivo

(A–C) High-pressure freezing (HPF) electron microscopy of the developing optic nerve. Overview of optic nerve cross sections from control and NR1 mutant mice at P10 (A), P20 (B), and P70 (C). At early and late stages, NR1 mutant nerves are indistinguishable from controls. A minor hypomyelination is apparent at P20. Scale bars, 0.5 μm (A and B) and 0.2 μm (C).

(D) Electron microscopy of conventionally fixed optic nerves from mutant and controls, with unmyelinated (U), ensheathed (E), and myelinated (M) axons. Scale bar, 1 μm.

(E–I) Axon size distribution and myelin sheath thickness (g-ratio) at P18 and P70.

(E) Diameter spectrum of myelinated axons with relatively more myelinated small caliber axons in control nerves than in NR1 cKO at P18 (***p < 0.001, two-way ANOVA, Bonferroni's post-test).

(F) Cumulative frequency of g-ratios (low to high) measured for individual optic nerves of each genotype. Note the significant shift to higher g-ratios in P18 NR1 mutants (inset: means ± SEM of all g-ratios for two axon size groups).

(G) At P18, myelinated (M) axons are transiently reduced in mutant optic nerves, unlike the number of unmyelinated (U) and merely ensheathed (E) axons (400–700 axons counted per nerve; n = 3, p = 0.048). (H and I) Axon size distribution (H) and optic nerve g-ratios (I) are similar in mutants and controls.
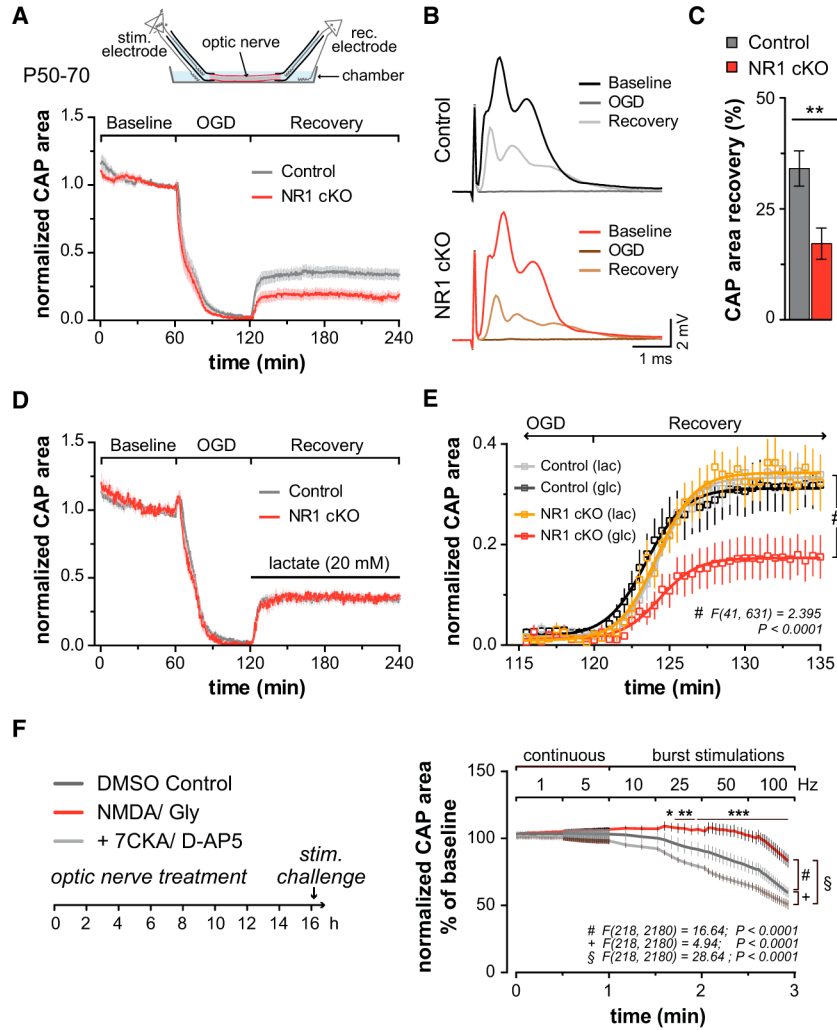
Figure 4. Axonal Energy Metabolism Regulated by NMDA Receptor and GLUT1-Dependent Lactate Export from Myelinating Oligodendrocytes

(A) Top: scheme of recording compound action potentials (CAPs) from acutely isolated optic nerves. After 1 hr, nerves were subjected to 60 min oxygen glucose deprivation (OGD) followed by reperfusion with ACSF containing 10 mM glucose. Bottom: optic nerve CAP areas (i.e., area underneath CAPs as shown in C) normalized to baseline. Note the rapid decline of nerve conduction and the incomplete recovery after reperfusion, which is more pronounced in NR1 mutants (red) compared to controls (black).

(B) Averaged optic nerve CAPs during baseline, OGD, and recovery phase in control (top) and NR1 cKO (bottom).

(C) Quantification of data in (A) with reduced functional recovery after OGD in mutants (n = 12) versus controls (n = 11, p = 0.0046, Student's t test).

(D) With 20 mM lactate, the functional recovery after OGD was the same in NR1 mutants (n = 6) and controls (n = 8).

(E) Axonal recovery at higher temporal resolution, comparing 10 mM glucose (glc) and 20 mM lactate (lac). Depicted are fitting curves (lines, Boltzmann fit) for the average CAP area over time (p < 0.0001, two-way ANOVA comparing glucose and lactate in NR1 mutants).

(F) Wild-type optic nerves, maintained functional ex vivo for 16 hr in the presence of NMDA/Gly (100 μM), or NMDA/Gly plus 7CKA/D-AP5 (100 μM), or only DMSO (control), were subsequently challenged with increasing stimulation frequencies. Note that nerves treated with NMDA/Gly show less decline of CAP area at higher frequency (p < 0.0001 two-way ANOVA with Dunnett's multiple comparisons test, n = 6 nerves for each treatment group).
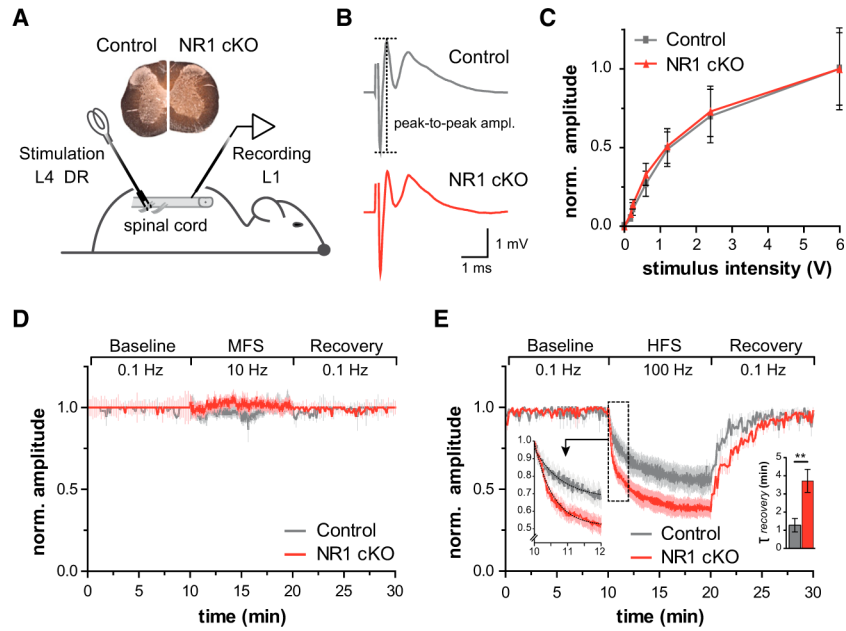
Figure 5. Requirement of Oligodendroglial NMDA Receptors for High-Frequency Conduction

(A) Scheme of stimulating DRG axons of lumbar segment L4 and recording from fasciculus gracilis at L1 (inset: intact myelination of spinal cord in mutants and controls, Gallya's stain).

(B) Representative CAPs (averaged) in control (top) and mutants at age 4–6 months. Dotted line: peak-to-peak amplitude used to analyze firing strength of fastest axon groups. Conduction delays were unchanged.

(C) Normal axonal excitability in mutants measured at increasing stimulus intensities with peak-to-peak amplitude normalized to maximal readings.

(D) After 10 min at 0.1 Hz, stimulation frequency increased to 10 Hz (medium frequency stimulation, MFS), showing no difference between mutants (n = 6) and controls (n = 3).

(E) 100 Hz (high frequency stimulation, HFS) caused a decrease of firing strength (within seconds) that was significantly faster and stronger in NR1 mutants (n = 7) than controls (n = 5). Left inset: higher temporal resolution for indicated region, $F_{interaction}$ (119, 1,190) = 3.07, p < 0.0001, two-way ANOVA). Right inset: slower recovery of CAPs at the end of HFS, monitored at 0.1 Hz (τ calculated from normalized exponential fits, p = 0.0084, Student's t test).
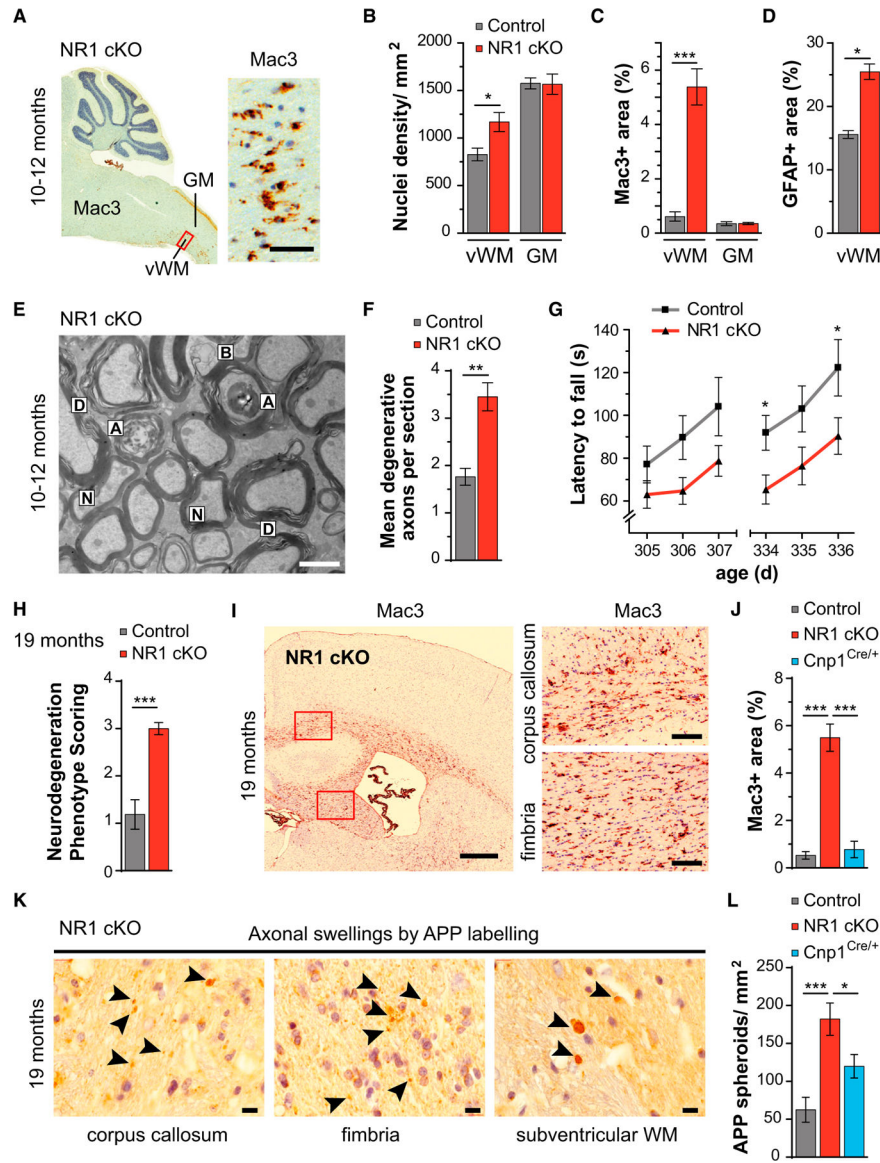
Figure 6. Late-Onset Neuroinflammation and Axonopathy in NR1 cKO Mice

(A) Indirect signs of neurodegeneration in white matter tracts at 1 year of age and overview (left) of sagittal cerebellum-spinal cord section from NR1 cKO mice. Signs of local inflammation (Mac3 immunostaining) were more obvious in the ventral white matter (vWM) compared to spinal cord gray matter (GM). Higher magnification (region marked by a red rectangle) reveals activated microglia (Mac3). Scale bar, 20 μm. See also Figure S7.

(B) Neuroinflammation in the ventral white matter of NR1 cKO mice confirmed by increased density of cell nuclei (p = 0.029, n = 4, Student's t test). In adjacent GM, nuclear densities are unaltered.

(C) Quantification of the Mac3^{+} immunostained area (microgliosis) in vWM of NR1 mutant mice (p = 0.0004, n = 4, Student's t test)

(D) Quantification of the GFAP[+] area (astrogliosis) in vWM of NR1 mutant mice (p = 0.013, Student's t test).

(E and F) By electron microscopy of ventral cervical spinal cord cross sections (E), ultrastructural features of axonal pathology and degeneration were more frequent in NR1 mutant mice compared to controls (F) (n = 4–5 mice with 12–14 randomly taken images, covering 530 μm^2 each, p = 0.0014, Student's t test). Scale bar, 2 μm. In (E): A, axonal degeneration; B, blebbing membranes; D, delamination; N, normal myelin.

(G) Motor deficits of NR1 cKO mutants at 10–11 months of age, demonstrated by Rotarod testing on three consecutive days (repeated the following month). The latency to fall is decreased in NR1 mutant mice (red line) compared to littermate controls ($F_{genotype}$ (1, 17) = 4.95, p = 0.040, n = 9–10, two-way ANOVA).

(H) At age 19 months, NR1 cKO mice (n = 11) display significant neurological deficits compared to controls (n = 8, p < 0.001 Student's t test). Clinical scores are 0, asymptomatic; 1, hind limb clasping; 2, additionally, hunchback visible; 3, additionally, frequent slipping while walking on grid; 3.5, additionally, failure to hold on inverted grid; 4, additionally, hind limb ataxia and unable to hold on upright grid; 4.5, spastic hind limbs.

(I) Brain sections of 19-month-old NR1 cKO mice immunostained for $Mac3^+$ show widespread signs of neuroinflammation in white matter tracts; corpus callosum and fimbria are magnified (right panel).

(J) Quantification of $Mac3^+$ immunostained area in NR1 mutants compared to littermate controls and age-matched Cnp1$^{Cre/+}$ mice (n = 4–6 mice, p < 0.001, linear mixed effects analysis with post hoc Tukey correction for multiple comparisons).

(K) Axonopathy in white matter tracts revealed by APP immunolabeling (arrow heads) in brain sections of 19-month-old NR1 cKO mice; corpus callosum, fimbria, and subventricular white matter are shown.

(L) Quantification of APP spheroids in NR1 mutants in comparison to littermate controls and age-matched Cnp1$^{Cre/+}$ mice (n = 4–6 mice; control versus NR1 cKO p < 0.001 and Cnp1$^{Cre/+}$ versus NR1 cKO p = 0.03, linear mixed effects analysis with post hoc Tukey correction for multiple comparisons).
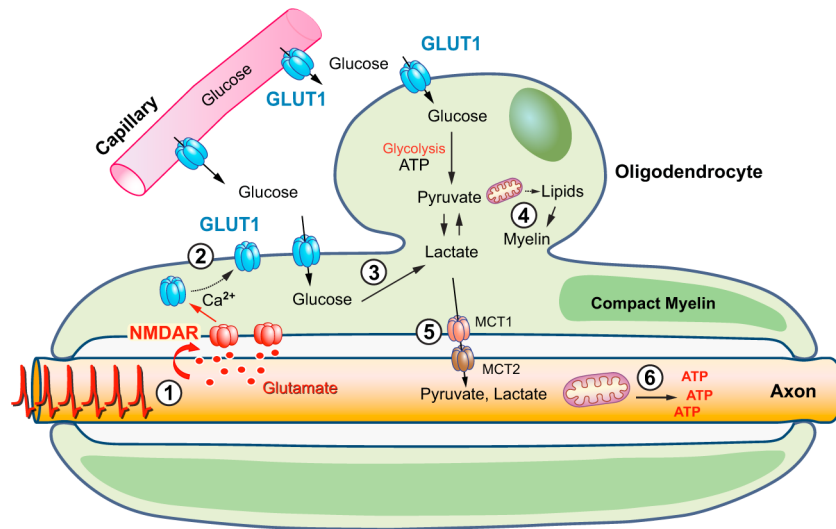
Figure 7. Schematic Depiction of Oligodendroglial NMDA Receptor Signaling
Working model in which axonal electrical activity in developing white matter tracts constitutes a glutamatergic signal for the surrounding OPC/oligodendrocytes/myelin compartments (1). After myelination, NMDA receptors associated with the internodal/paranodal membrane respond to axonal glutamate release as a surrogate marker for increased axonal electrical activity and energy needs, causing (2) the incorporation of additional glucose transporters into oligodendrocytes and myelin and the adaptation of glucose uptake (feed-forward regulation). Glycolysis products (3) are initially used for ATP and lipid synthesis (4). Later, mature oligodendrocytes release lactate (or pyruvate) to fuel the axonal compartment (5) for mitochondrial ATP production (6). Regulation of oligodendroglial glucose uptake by axonal energy needs could help prevent abnormal accumulation of lactate. The possible effect of glutamate on glucose transporters on astrocytes is not shown.